**Original Article**

# Role of Nb on the phase stability and morphology of Ti−Ni−Cu−Nb alloys

Jessica Dornelas Silva [a,*], Gisele Fernandes Chaves Macieira [a],
Dilson Silva dos Santos [b], Leandro de Arruda Santos [a],
Vicente Tadeu Lopes Buono [a]

[a] Department of Metallurgical and Materials Engineering, Universidade Federal de Minas Gerais (UFMG), Belo Horizonte, MG, Brazil
[b] Department of Metallurgical and Materials Engineering, Universidade Federal Do Rio de Janeiro (UFRJ), Rio de Janeiro, RJ, Brazil

## ARTICLE INFO

## ABSTRACT

$Ti_{52-x}Ni_{38}Cu_{10}Nb_x$ alloys with Nb additions of x = 4, 6, and 10 at.% were produced through arc melting. The phase constitution and morphology were evaluated through X-ray diffraction, microstructural analyses (scanning electron microscopy/energy-dispersive X-ray spectroscopy), and thermodynamic calculations (ThermoCalc). The as-cast alloys exhibited a TiNi matrix, β-Nb/TiNi eutectic, and $Ti_2Ni$ precipitates. Under equilibrium conditions, TiNi and a small fraction of β-Nb were expected. Increasing the Nb content resulted in a higher β-Nb volume fraction, development of different morphologies for $Ti_2Ni$ precipitates, and formation of Ti particles. The Scheil calculator and virtual composition of the liquid were used to simulate the effect of chemical segregation during solidification. We demonstrated that the metastable phases formed during solidification and the Nb content played a vital role in the solidification sequence, phase distribution, and morphology of the alloy.

## 1. Introduction

The addition of copper as a substitute for nickel in binary TiNi shape memory alloys is known to result in ternary alloys with narrow thermal and stress transformation hysteresis, low composition sensitivity of the transformation temperatures, and increased damping capacity in comparison to binary TiNi alloys. These characteristics can be associated with improved structural and functional fatigue properties during superelastic cycling, which makes them suitable for a wide range of new applications [1,2]. Adding a quaternary element is one of the ways of adjusting the required properties and martensitic transformation temperatures for new potential applications such as solid-state refrigeration [3−11].

Among various quaternary additions, Nb has been reported to increase the ductility of ternary Ti−Ni−Cu alloys through the introduction of the soft β-phase [12,13] and to decrease their direct and reverse martensitic transformation temperatures [13,14]. Previous studies on this quaternary system have

---

demonstrated that Ti−Ni−Cu−Nb alloys exhibit good mechanical properties [12,15] and predominant B2↔B19 phase transformation [13,14], which is characterized by an intrinsically lower hysteresis than that of B2↔B19′ [2]. Their properties and characteristic transformation temperatures have been reported to be influenced by Nb content [13,14] and heat-treatment conditions [12], providing powerful tools for alloy optimization. Furthermore, the addition of Nb into $Ti_{54}Ni_{34}Cu_{12}$ was reported to significantly enhance the thermal cycling stability of this alloy [16].

While formability is favored by the increased ductility resulting from the presence of the soft β-phase, the ability to control the reversible transformation temperature and the stabilization of the low hysteresis B2↔B19 phase transformation can be highlighted. These results suggest that there is potential to develop formable TiNiCuNb alloys that could be suitable for room temperature applications requiring high functional and mechanical stability during superelastic cycling.

However, only few studies have been conducted on this quaternary system and the effect of addition of Nb on the ternary Ti−Ni−Cu system thermodynamics and solidification microstructure are yet to be explored. Therefore, this study aims to understand the role of Nb in the phase stability of Ti−Ni−Cu−Nb alloys through thermodynamic calculations and microstructural analyses. Based on the binary phase diagram analysis [17−24] and the isomorphous Ti−Nb interactions at high temperatures [21], quaternary alloys were produced by adding Nb as a substitute for Ti in the $Ti_{52}Ni_{38}Cu_{10}$ base alloy.

## 2. Experimental procedure

$Ti_{52-x}Ni_{38}Cu_{10}Nb_x$ alloys were synthesized with Nb additions of x = 4, 6, and 10 at%, hereafter referred to as Nb4, Nb6, and Nb10, respectively. Thermodynamic simulations using ThermoCalc (2018b) software were used to predict the equilibrium microstructures using the TCNI8 (v8.1) database.

Melting was performed from elemental constituents (>99.5% purity) into 30 g ingots in an arc-melting furnace. This procedure was performed under an argon-controlled atmosphere in a water-cooled copper mold. Each ingot was remelted at least six times to ensure chemical homogeneity, being turned over after each melting/solidification step. A new Nb10 sample was cast and homogenized for 24 h at 900 °C to achieve close-to-equilibrium conditions in the alloy with the highest Nb content. Slow cooling took place inside of the furnace.

Samples from the as-cast and homogenized alloys were cut, mounted, ground, and mechanically polished for microstructural evaluation through scanning electron microscopy (SEM)/energy-dispersive X-ray spectroscopy (EDS) (FEI Inspect S50) with backscattered electrons. X-ray diffraction (XRD) was used for phase identification in a PANalytical Empyrean diffractometer with Cu K-α radiation, with 2θ ranging from 30 to 110°, at a scan speed of 0.02°/s. Materials Project database was used for peak indexation based on the phases reported in previous studies [12−15,25−27]. The relative integrated peak areas were used to qualitatively compare the phase fractions of the different alloys.

Differential scanning calorimetry (DSC; Shimadzu - DSC60) was used to assess the reversible martensitic transformation of the as-cast alloy. The specimens were cooled to −100 °C and subsequently heated at 20 °C/min to 100 °C. Cooling to −100 °C occurred at the same rate as the heating. This heating/cooling cycle was repeated five times to acquire information on thermal cycling stability.

## 3. Results

### 3.1. Equilibrium simulations

The $Ti_{52-x}Ni_{38}Cu_{10}Nb_x$ system was initially assessed using its pseudobinary phase diagram, as shown in Fig. 1(a). The volume fractions of the equilibrium phases as a function of
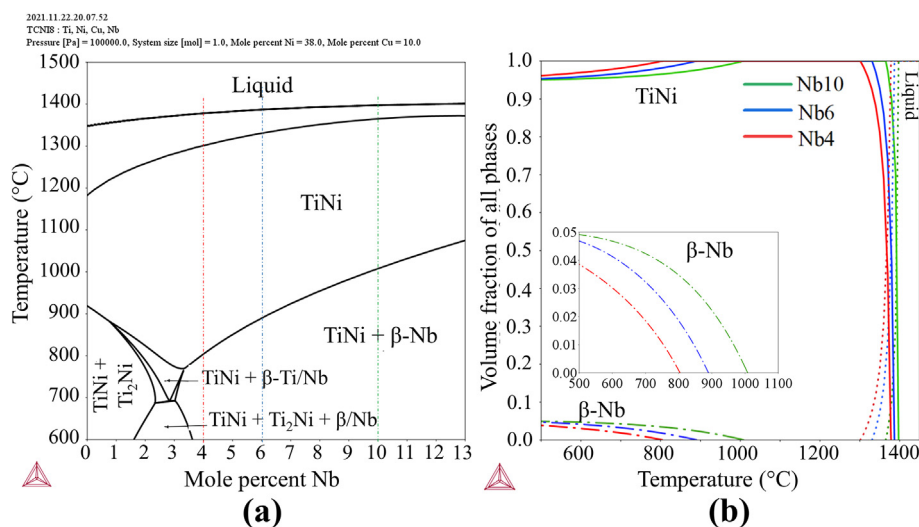


Fig. 1 − (a) $Ti_{52-x}Ni_{38}Cu_{10}Nb_x$ pseudobinary phase diagram and (b) volume fractions of stable phases with varying temperatures under equilibrium conditions for x = 4, 6, 8, and 10 at%.
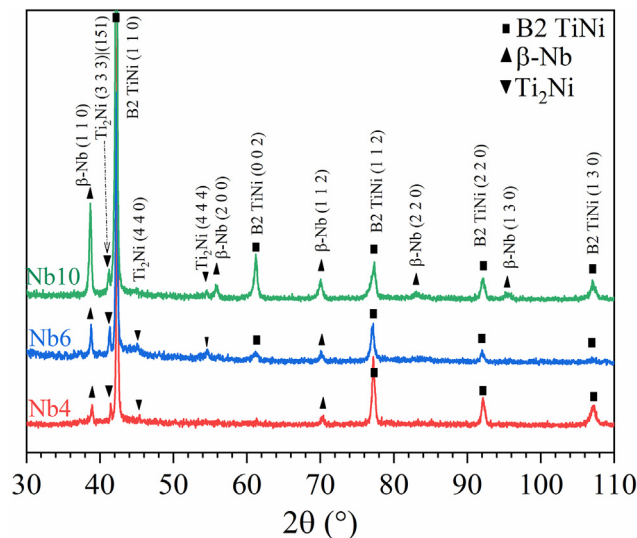
**Fig. 2 – XRD spectra of the as-cast alloys.**

temperature in the selected alloys, marked in Fig. 1(a), were obtained using the equilibrium calculator and are illustrated in Fig. 1(b). Nb4 is represented by red lines, Nb6 by blue lines, and Nb10 by green lines. The different dashed lines represent the different phases illustrated in Fig. 1(b). Under these conditions, all cast alloys should solidify as pure TiNi, and as much as 5vol% of β-Nb could precipitate during slow cooling.

### 3.2.    Microstructural evaluation and phase identification in the as-cast alloys

The XRD spectra of the as-cast alloys are illustrated in Fig. 2. The B2 type TiNi (MP #571) austenitic phase was identified, whereas β-Nb (MP #75) and $Ti_2Ni$ (MP #1808) peaks were present in all compositions.
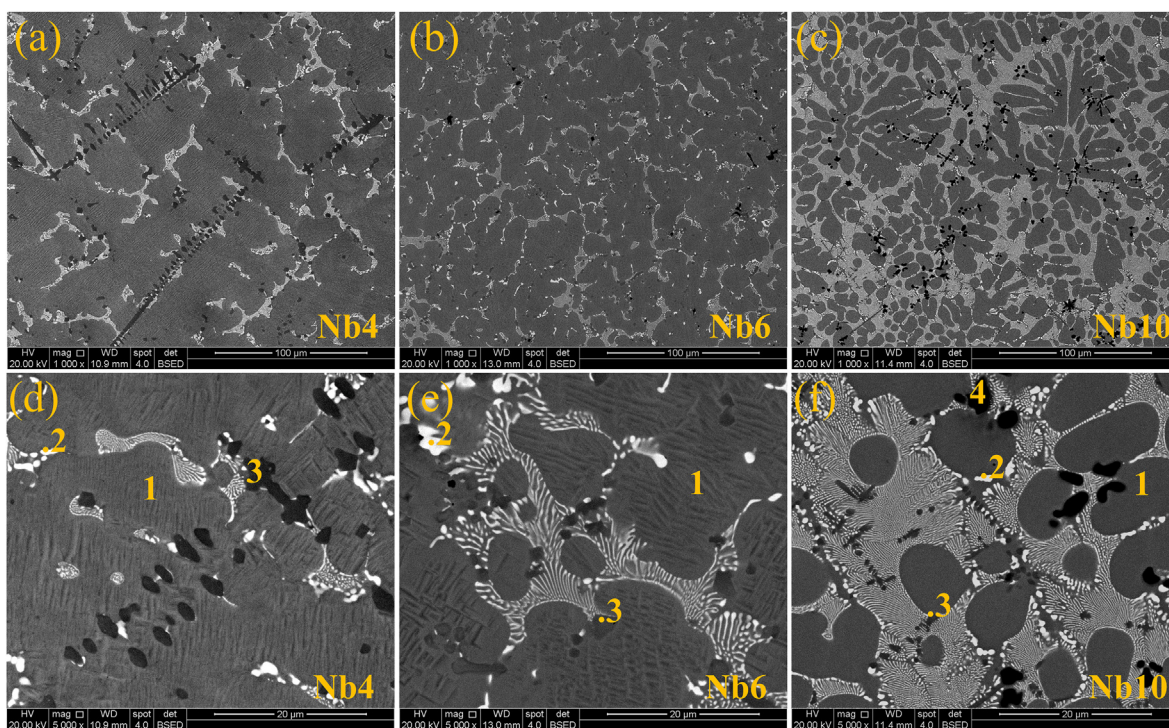


**Fig. 3 – Backscattered electron images of (a,b) Nb4, (c,d) Nb6, (e,f) Nb8, and (g,h) Nb10 alloy at (a,b,c) 1000× and (d,e,f) 5000× magnifications.**

**Table 1 — Mean element contents measured on the EDS semi-quantitative analysis of different phases in Nb4, Nb6, Nb8, and Nb10 as-cast alloys. Values are in atomic percent.**

|  |  | Ti (at%) | Ni (at%) | Cu (at%) | Nb (at%) |
|---|---|---|---|---|---|
| TiNi | Nb4 | 46.5 ± 0.3 | 41.7 ± 0.8 | 9.0 ± 0.9 | 2.7 ± 0.1 |
|  | Nb6 | 45.0 ± 0.6 | 41.2 ± 1.6 | 9.8 ± 1.6 | 3.7 ± 0.5 |
|  | Nb10 | 44.3 ± 0.5 | 42.9 ± 0.6 | 8.1 ± 0.5 | 4.6 ± 0.3 |
| β-Nb | Nb4 | 34.8 ± 2.0 | 9.0 ± 4.3 | 4.5 ± 1.4 | 51.7 ± 6.6 |
|  | Nb6 | 22.7 ± 2.0 | 7.1 ± 2.0 | 3.8 ± 0.8 | 64.7 ± 6.6 |
|  | Nb10 | 23.1 ± 2.7 | 10.3 ± 1.9 | 5.1 ± 1.0 | 61.5 ± 5.5 |
| Ti₂Ni | Nb4 | 62.3 ± 0.2 | 30.2 ± 0.6 | 3.7 ± 0.1 | 3.8 ± 0.3 |
|  | Nb6 | 56.4 ± 1.9 | 30.8 ± 0.7 | 4.6 ± 0.6 | 8.2 ± 1.9 |
|  | Nb10 | 52.8 ± 1.2 | 31.0 ± 0.1 | 6.0 ± 0.7 | 10.2 ± 0.9 |
| Ti | Nb10 | 90.1 ± 2.7 | 3.4 ± 1.8 | 1.4 ± 0.5 | 5 ± 0.6 |

Backscattered electron images of the as-cast samples obtained using SEM are shown in Fig. 3. EDS analysis (Table 1) was used to identify the phases based on the XRD results. The gray matrix phase, indexed as number 1, was identified as the TiNi phase. The white phase, number 2, is an Nb-rich phase identified as β-Nb in the XRD spectra. The dark gray phase, number 3, was identified as the Ti₂Ni intermetallic. Additionally, the black particles, number 4, exhibited over 90 at% Ti, suggesting that it is metallic Ti. This phase was not identified in the XRD pattern, probably due to the small amounts of the precipitates and/or overlapping peaks of other phases present at higher fractions.

β-Nb was mainly observed in a lamellar eutectic constituent with the TiNi phase. Its volume fraction, obtained by dividing the integrated peak areas of this phase by the sum of all the integrated peak areas in the XRD pattern, increased with increasing Nb content:15, 23, and 31% were observed in Nb4, Nb6, and Nb10 alloys, respectively. Ti₂Ni exhibited different morphologies and distributions as a function of the alloy composition. In Nb4, a dendritic-like morphology was observed. In Nb6, prismatic precipitates were observed within the matrix phase and associated with the β-Nb phase

and the eutectic structure. In Nb10, the Ti₂Ni precipitates were mainly intercalated with the β-Nb/TiNi eutectic constituent. Metallic Ti was not observed in Nb4; however, it was noteworthy in the Nb10 alloy, where it appeared in relatively high amounts as dendrites.

### 3.3. Effect of homogenization on the Nb10 as-cast microstructure

The Nb10 alloy was selected for the homogenization treatment such that it would be possible to observe the effect of this heat treatment on all the identified second phases, namely β-Nb, Ti₂Ni, and Ti. After homogenization, the phase constitution of the as-cast alloy was maintained, as shown in Fig. 4.

Partial coalescence of the β-Nb lamellae and Ti₂Ni particles was observed, as shown in Fig. 4(a). By comparing with the as-cast microstructure, it appears that Ti₂Ni precipitates formed and coalesced around the Ti particles, as indicated by the arrow. There were also regions, as shown in Fig. 4(b), where no apparent second-phase coalescence occurred. In turn, fine precipitation within the TiNi matrix was observed both in regions with high and low second-phase coalescence, as highlighted by the rectangles. The contrast of these precipitates in the backscattered analysis suggests that they are also Nb-rich.

### 3.4. DSC analysis

The Nb6 alloy, with an intermediate Nb content, was selected for thermal stability analyses. The DSC chart obtained during the thermal cycling of this alloy, as illustrated in Fig. 5, showed a stable transformation behavior. It exhibited an austenitic finishing temperature (Af) less than, but close to room temperature, favoring further superelastic cycling. With thermal cycling, Af varied from 13.7 °C in the first cycle to 14.3 °C in the fifth cycle, as obtained from the tangent line method. Variations of 1.2 °C and 0.4 °C were observed on the direct and reverse martensitic transformation peak temperatures, respectively.



**(a)**                    **(b)**
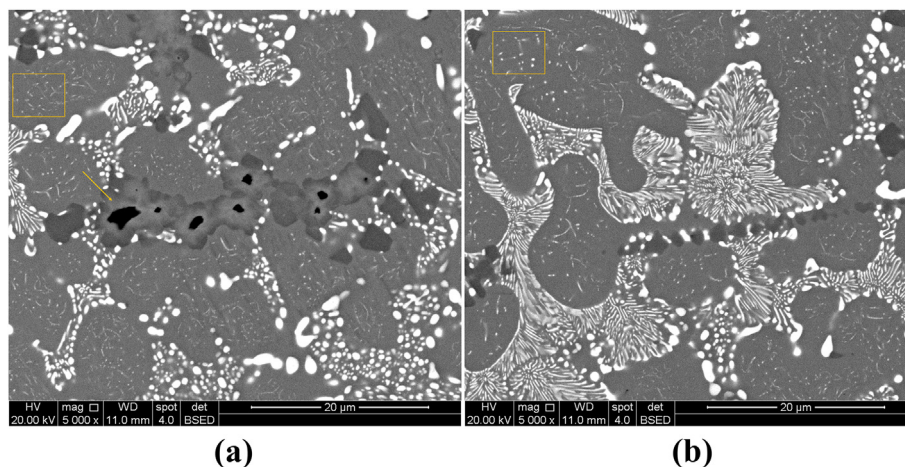
**Fig. 4 — Backscattered electron images obtained in the SEM analyses in different regions of the homogenized Nb10 alloy at 5000× magnification.**
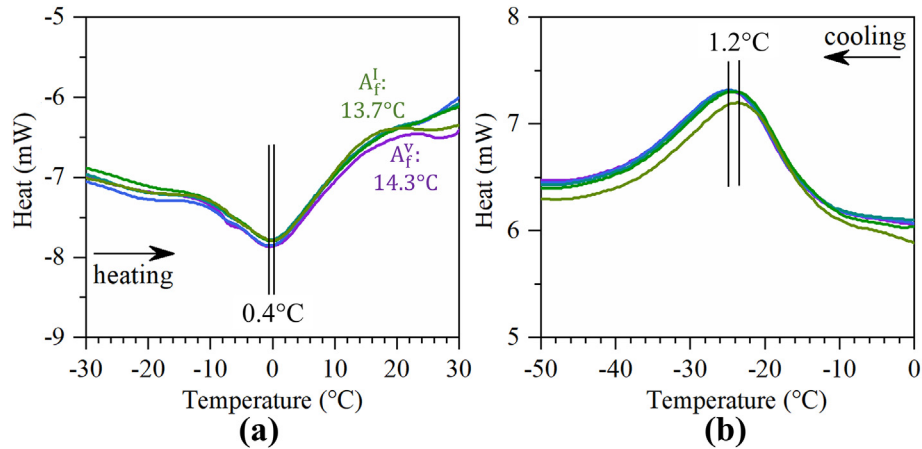
**Fig. 5 − DSC chart for the thermal cycle test of as-cast Nb6 alloy during (a) heating and subsequent (b) cooling.**

## 4.    Discussion

From conventional thermodynamic calculations (Fig. 1), TiNi and β-Nb are the equilibrium phases for all the cast alloys. However, these alloys also exhibited Ti$_2$Ni intermetallic phase, as in Ti-rich TiNi alloys. β-Nb and Ti$_2$Ni particles exhibited stable behavior during homogenization. At a temperature where no Ti$_2$Ni is thermodynamically expected, this phase coalesced rather than dissolving. The metallic Ti observed in the Nb10 alloy was partially dissolved to form Ti$_2$Ni during the homogenization treatment. The fine precipitation formed within the TiNi matrix phase in the homogenized sample appears to be β-Nb, which resulted from a supersaturation of Nb on the TiNi matrix.

The morphology and distribution of the β-Nb and Ti$_2$Ni phases in the as-cast microstructures suggested that they formed during solidification. The coalescence of these phases during homogenization, in turn, implies that local equilibrium conditions have been reached, resulting in a stable microstructure. Based on these results and discussions, the Scheil calculator was used to predict the phases formed during solidification. In this calculation, the equilibrium chemical composition of the solid phases formed at varying temperatures is considered, whereas diffusion is only expected to occur in the liquid.

In Fig. 6, the solid phases in equilibrium with the liquid are presented as functions of temperature and solid fraction. The results are in qualitative agreement with the observed microstructure: solidification starts with the formation of the TiNi matrix, whereas the β-phase and the Ti$_2$Ni intermetallic phase are predicted in the final stages. The solidification process is concluded by the occurrence of a eutectic reaction in all the alloys. In Nb4 and Nb6, Ti$_2$Ni solidification occurs
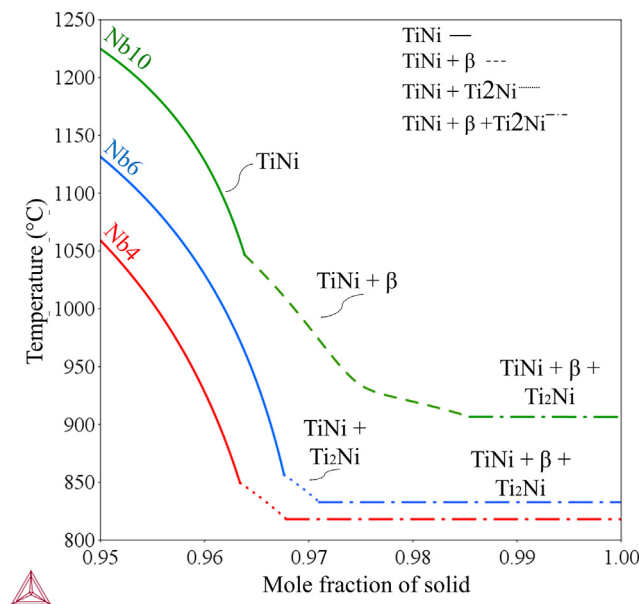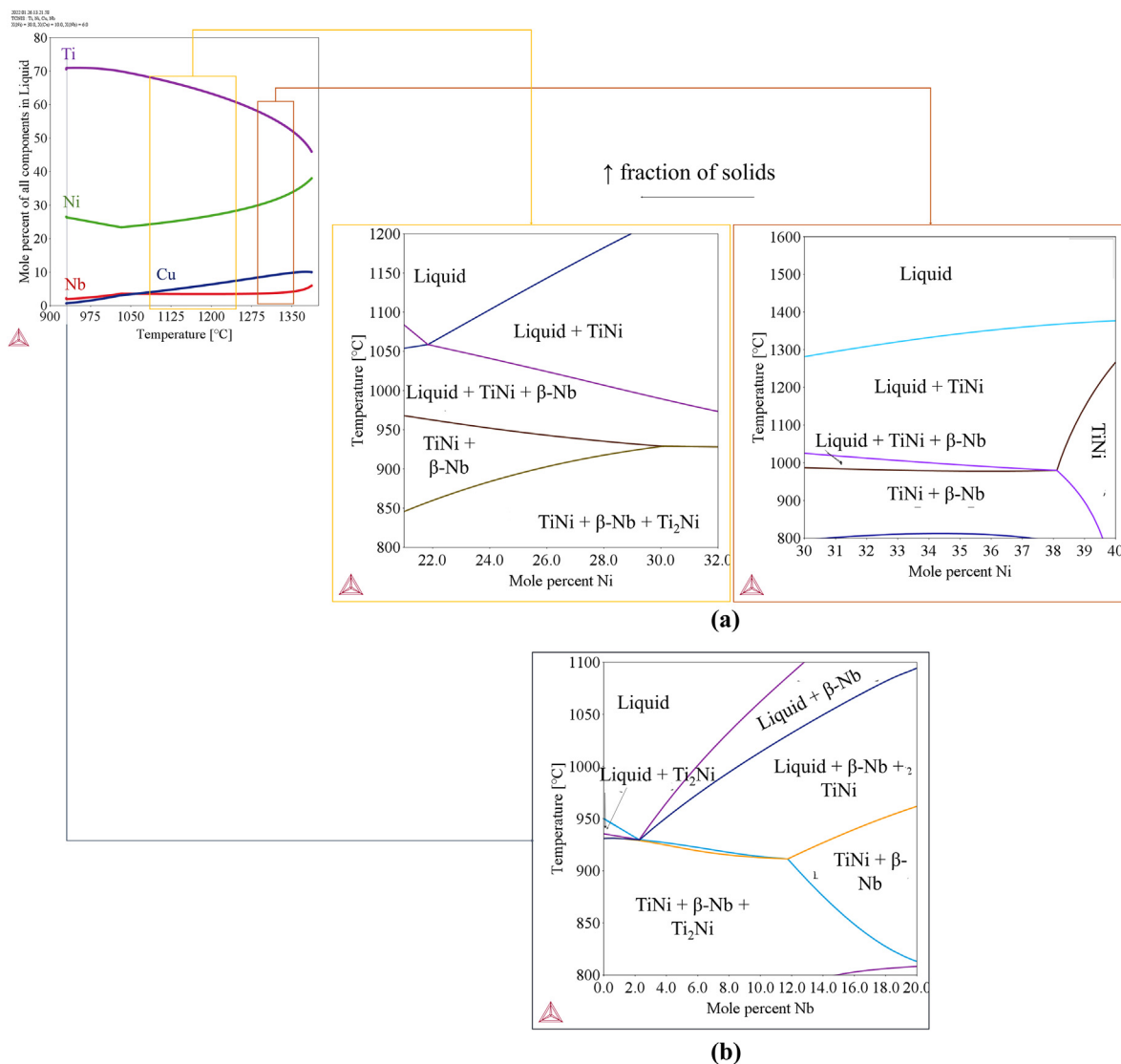


**Fig. 6 − Simulation of solidification using the Scheil calculator.**

**Fig. 7 – Equilibrium analyses of (a) TiNi pseudobinary with fixed Nb and Cu contents at different stages of solidification and (b) TiNb pseudobinary with fixed Ni and Cu contents on the final stages of solidification.**

before the eutectic reaction, being favored in the alloy with a lower Nb content. In Nb10, the β-phase appears first. The eutectic temperature is related to the presence of all these three phases in equilibrium with the liquid. Because it is a quaternary system, a reaction taking place at a constant temperature implies a four-phase reaction, L → TiNi + β + Ti$_2$Ni.

It is worth pointing out that the presence of Ti dendrites was observed in Nb10. The formation of the BCC β-phase outside of the eutectic was predicted in the Scheil calculation of this alloy. This β-phase can contain varying amounts Ti and Nb, and it is possible that of β-Ti formed directly from the liquid with dendritic morphology.

Considering that cooling takes place out-of-equilibrium, possibly leading to high chemical segregation when solid phases are formed, further analyses on the equilibrium phases that take place were performed. Virtual liquid compositions at varying temperatures for the Nb6 alloy, obtained via Scheil calculations, were used in the equilibrium calculator to

obtain pseudobinary diagrams considering the tendencies observed in the liquid composition variation. Under 90% solid formation, Ti–Ni pseudobinaries were analyzed with fixed Nb and Cu contents at different stages (Fig. 7(a)). In this region, the formation of the three-phase L → β + TiNi eutectic succeeding the pre-eutectic formation of TiNi is expected, even within the TiNi + liquid region shown in Fig. 6.

In the final stages (Fig. 7(b)), where the calculated Ni and Cu contents were relatively low and fixed, a Ti–Nb pseudobinary was analyzed such that the partition of Ti and Nb in a liquid enriched in these elements could be assessed. It was observed that the formation of Ti$_2$Ni can occur in different ways. At low Nb contents, it forms individually from the liquid and is succeeded by the occurrence of a four-phase L → TiNi + β + Ti$_2$Ni eutectic reaction. At intermediate Nb contents, it occurs only in the four-phase eutectic reaction after the formation of the β-phase and three-phase L → TiNi + β reaction. In turn, at high Nb contents, Ti$_2$Ni does not form, and only a three-phase eutectic is observed. These results are consistent with the
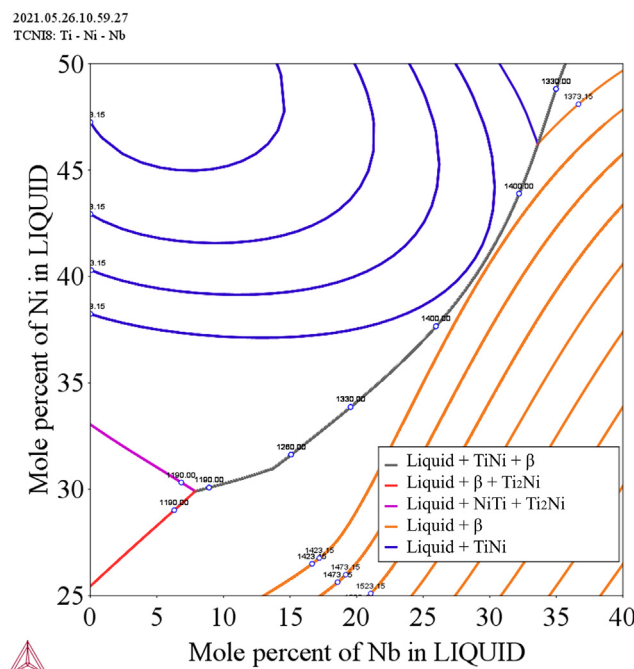
**Fig. 8 − Liquidus projection of ternary Ti−Ni−Nb.**

different morphologies observed for this phase in the microstructural analysis of Nb6, where it appeared within the TiNi matrix in association with the TiNi + β eutectic constituent.

The Ti−Nb pseudobinary represented in Fig. 7(b) can also be used to interpret the microstructure of Nb4 and Nb10 alloys. In Nb4, $Ti_2Ni$ exhibited a dendritic-like morphology because it was formed from the liquid phase. In Nb10, $Ti_2Ni$ was only observed intercalated with the TiNi + β eutectic constituent, which was predominant in relation to the three-phase TiNi/β-Nb/$Ti_2Ni$ eutectic. In this alloy, metallic Ti was observed as dendrites, also formed from the liquid phase. These results indicate that higher amounts of Nb hinder the formation of the $Ti_2Ni$ intermetallic by stabilizing β-Ti.

This behavior is closely related to the Ni−Ti−Nb ternary system, whose liquid projection, illustrated in Fig. 8, shows the formation of different three-phase and four-phase eutectic reactions involving the TiNi, β, and $Ti_2Ni$ phases. In alloys with higher Nb contents and, thus, higher Nb enrichments in the liquid, the formation of the β phase and three-phase L → TiNi + β reaction are favored, leading to the presence of β-Ti and higher fractions of TiNi + β-Nb lamellae. In contrast, alloys with lower Nb contents exhibited a favored formation of $Ti_2Ni$, which was also embedded in the TiNi matrix, while no β-Ti was observed.

Therefore, the phases obtained in the as-cast alloys were observed in the equilibrium phase diagrams when chemical segregation during solidification was considered. Furthermore, the different morphologies and distributions observed are consistent with the different cooling sequences in these calculations and were directly related to the Nb content of the alloy. The resultant microstructure exhibited high stability because local equilibrium was reached, and metastable

second phases were not easily dissolved, as indicated by the homogenized microstructure.

Although the produced alloys presented a complex microstructure constituted by metastable phases that were not dissolved during homogenization, the TiNi martensitic transformation promoted in the calorimetric test of the as-cast alloy exhibited high reproducibility. Because higher changes in transformation temperatures are expected to occur within the initial thermal cycles in TiNi alloys [28−32], the reproducibility observed in the martensitic transformation of the alloy indicates a high thermal stability.

An Af less than, but close to room temperature, obtained for the Nb6 alloy indicates that superelastic behavior may be achieved at room temperature. Therefore, the results achieved for the as-cast microstructure indicate the potential of alloys with stable room-temperature superelasticity.

## 5. Conclusions

In this study, $Ti_{52-x}Ni_{38}Cu_{10}Nb_x$, x = 4, 6, and 10 at% alloys were produced, and the effect of Nb on the phase stability was evaluated using microstructural analyses and thermodynamic simulations. All the cast alloys were composed of a matrix TiNi phase, a eutectic TiNi/β-Nb constituent, and $Ti_2Ni$ precipitates. Despite not being expected from ideal equilibrium conditions, β-Nb and $Ti_2Ni$ can be formed during solidification owing to chemical segregation: the former, in eutectic reactions, and the latter, embedded in the TiNi matrix or within a four-phase eutectic constituent. The morphology of the Ti-rich intermetallic was associated with the Nb content of the alloy and Ti/Nb partition on the liquid.

A higher Nb content seemed to hinder the formation of $Ti_2Ni$, and metallic Ti was also observed in Nb10. This phase constitution exhibited stable behavior during homogenization treatment, which was related to the development of local equilibrium conditions.

## Declaration of Competing Interest

The authors declare that they have no known competing financial interests or personal relationships that could have appeared to influence the work reported in this paper.

## Acknowledgments

REFERENCES

[1] Nam TH, Saburi T, Shimizu K. Cu-content dependence of shape memory characteristics in Ti-Ni-Cu alloys. Mater Trans, JIM 1990;31. https://doi.org/10.1063/1.5030626.

[2] Otsuka K, Wayman CM. Shape memory materials. Cambridge: Cambridge University Press; 1998.

[3] Wieczorek A, Frenzel J, Schmidt M, Seelecke S, Eggeler G, Maaß B, et al. Optimizing Ni—Ti-based shape memory alloys for ferroic cooling. Funct Mater Lett 2017;10:1—8. https://doi.org/10.1142/S179360471740001X.

[4] Bruederlin F, Bumke L, Chluba C, Ossmer H, Quandt E, Kohl M. Elastocaloric cooling on the miniature scale: a review on materials and device engineering. Energy Technol 2018:1588—604. https://doi.org/10.1002/ente.201800137.

[5] Schmidt M, Ullrich J, Wieczorek A, Frenzel J, Schutze A, Eggeler G, et al. Thermal stabilization of NiTiCuV shape memory alloys: observations during elastocaloric training platform that allows observation of temperature profiles. Shape Mem Superelasticity 2015;1:132—41. https://doi.org/10.1007/s40830-015-0021-4.

[6] Yang Z, Cong D, Yuan Y, Li R, Zheng H, Sun X, et al. Large room-temperature elastocaloric effect in a bulk polycrystalline Ni-Ti-Cu-Co alloy with low isothermal stress hysteresis. Appl Mater Today 2020;21:100844. https://doi.org/10.1016/j.apmt.2020.100844.

[7] Chen H, Xiao F, Liang X, Li Z, Li Z, Jin X, et al. Giant elastocaloric effect with wide temperature window in an Al-doped nanocrystalline Ti—Ni—Cu shape memory alloy. Acta Mater 2019;177:169—77. https://doi.org/10.1016/j.actamat.2019.07.033.

[8] Frenzel J, Wieczorek A, Opahle I, Maaß B, Drautz R, Eggeler G. On the effect of alloy composition on martensite start temperatures and latent heats in Ni — Ti-based shape memory alloys. Acta Mater 2015;90:213—31. https://doi.org/10.1016/j.actamat.2015.02.029.

[9] Li J, Yi X, Sun K, Sun B, Gao W, Wang H, et al. The effect of Zr on the transformation behaviors, microstructure and the mechanical properties of Ti-Ni-Cu shape memory alloys. J Alloys Compd 2018;747:348—53. https://doi.org/10.1016/j.jallcom.2018.03.053.

[10] Yi X, Wang H, Gao W, Sun B, Niu X, Meng X, et al. Control of microstructural characteristics and martensitic transformation behavior of Ti—Ni—Cu alloys by Pt doping. J Alloys Compd 2019;802:181—9. https://doi.org/10.1016/j.jallcom.2019.06.217.

[11] Lemke JN, Gallino F, Cresci M, Zilio S, Coda A. Low-hysteresis shape memory alloy scale-up: Dsc, xrd and microstructure analysis on heat-treated vacuum induction melted Ni-Ti-Cu-Pd alloys. Metals 2021;11. https://doi.org/10.3390/met11091387.

[12] Jiang D, Liu Y, Liu W, Song L, Jiang X, Yanh H, et al. Microstructure, transformation behavior and mechanical properties of a (Ti50Ni38Cu12)93Nb7 alloy. Mater Sci Eng, A 2015;627:348—50. https://doi.org/10.1016/j.msea.2015.01.028.

[13] Wang GC, Hu KP, Tong YX, Tian B, Chen F, Li L, et al. Influence of Nb content on martensitic transformation and mechanical properties of TiNiCuNb shape memory alloys. Intermetallics 2016;72:30—5. https://doi.org/10.1016/j.intermet.2016.01.009.

[14] Liu MY, Qi WY, Tong YX, Tian B, Chen F, Li L. Study of martensitic transformation in TiNiCuNb shape memory alloys using dynamic mechanical analysis. Vacuum 2018;155:358—60. https://doi.org/10.1016/j.vacuum.2018.06.040.

[15] Li J, Wang H, Liu J, Ruan J. Effects of Nb addition on microstructure and mechanical properties of TiNiNb alloys fabricated by elemental powder sintering. Mater Sci Eng, A 2014;609:235—40. https://doi.org/10.1016/j.msea.2014.05.007.

[16] Tong Y, Gu H, James RD, Qi W, Shuitcev AV, Li L. Novel TiNiCuNb shape memory alloys with excellent thermal cycling stability. J Alloys Compd 2019;782:343—7. https://doi.org/10.1016/j.jallcom.2018.12.219.

[17] ASM International. ASM handbook volume 3: alloy phase diagrams. 1998.

[18] Otsuka K, Ren X. Physical metallurgy of Ti—Ni-based shape memory alloys. Prog Mater Sci 2005;50:511—678. https://doi.org/10.1016/j.pmatsci.2004.10.001.

[19] Murray JL. The Cu-Ti (copper-titanium) system. Bull Alloy Phase Diagrams 1983;4:81—95.

[20] Moffat DL, Kattner UR. Stable and metastable Ti-Nb phase diagrams. Metall Trans A, Phys Metall Mater Sci 1988;19:2389—97. https://doi.org/10.1007/BF02645466.

[21] Murray JL. The Nb-Ti (niobium-titanium) system. Bull Alloy Phase Diagrams 1981;2:55—61.

[22] Kejun Z, Xianzhang Z, Zhanpeng J. A thermodynamic calculation of the Ni-Nb phase diagram. J Alloys Compd 1992;179:177—85. https://doi.org/10.1016/0925-8388(92)90217-W.

[23] Bolcavage A, Kattner UR. A reassessment of the calculated Ni-Nb phase diagram. J Phase Equil 1996;17:92—100. https://doi.org/10.1007/BF02665782.

[24] Hamalainen M, Jaaskelainen K, Luoma R, Nuotio M, Taskinen P, Teppo O. A thermodynamic analysis of the binary alloy systems Cu-Cr, Cu-Nb, Cu-V. Calphad 1990;14:125—37.

[25] Piao M, Miyazaki S, Otsuka K, Nishida N. Effects of Nb addition on the microstructure of Ti-Ni alloys. Mater Trans, JIM 1992;33:3337—45.

[26] Tong YX, Jiang PC, Chen F, Tian B, Li L, Zheng YF, et al. Microstructure and martensitic transformation of an ultrafine-grained TiNiNb shape memory alloy processed by

equal channel angular pressing. Intermetallics 2014;49:81—6. https://doi.org/10.1016/j.intermet.2014.01.019.

[27] Zheng HX, Mentz J, Bram M, Buchkremer HP, Stöver D. Powder metallurgical production of TiNiNb and TiNiCu shape memory alloys by combination of pre-alloyed and elemental powders. J Alloys Compd 2008;463:250—6. https://doi.org/10.1016/j.jallcom.2007.09.081.

[28] Miyazaki S, Imai T, Igo Y, Otsuka K. Effect of cyclic deformation on the pseudoelasticity characteristics of Ti-Ni alloys. Metall Trans A, Phys Metall Mater Sci 1986;17:115—20. https://doi.org/10.1007/BF02644447.

[29] Mendes Rodrigues MC, Corrêa Soares G, Lopes Buono VT, de Arruda Santos L. Effects of pseudoelastic cycling under different temperatures on physical and mechanical properties of a NiTi alloy. Adv Sci Technol 2016;97:134—40. https://doi.org/10.4028/www.scientific.net/ast.97.134.

[30] Eggeler G, Hornbogen E, Yawny A, Heckmann A, Wagner M. Structural and functional fatigue of NiTi shape memory alloys. Mater Sci Eng, A 2004;378:24—33. https://doi.org/10.1016/j.msea.2003.10.327.

[31] Urbina C, De la Flor S, Ferrando F. Effect of thermal cycling on the thermomechanical behaviour of NiTi shape memory alloys. Mater Sci Eng, A 2009;501:197—206. https://doi.org/10.1016/j.msea.2008.10.026.

[32] Uchil J, Kumara KG, Mahesh KK. Effect of thermal cycling on R-phase stability in a NiTi shape memory alloy. Mater Sci Eng, A 2002;332:25—8. https://doi.org/10.1016/S0921-5093(01)01711-7.